JPhys Materials

PAPER • OPEN ACCESS

Very high upper critical fields and enhanced critical current densities in Nb_3Sn superconductors based on Nb–Ta–Zr alloys and internal oxidation

To cite this article: F Buta *et al* 2021 *J. Phys. Mater.* **4** 025003

Journal of Physics: Materials

PAPER

Very high upper critical fields and enhanced critical current densities in Nb_3Sn superconductors based on Nb–Ta–Zr alloys and internal oxidation

F Buta[1], M Bonura[1], D Matera[1], G Bovone[1], A Ballarino[2], S C Hopkins[2], B Bordini[2], X Chaud[3] and C Senatore[1]

[1] University of Geneva, DQMP, Geneva, Switzerland
[2] European Organization for Nuclear Research CERN, Geneva, Switzerland
[3] French National High Magnetic Field Laboratory, Grenoble, France

E-mail: florin.buta@unige.ch

OPEN ACCESS

RECEIVED
20 December 2020

REVISED
5 February 2021

ACCEPTED FOR PUBLICATION
15 February 2021

PUBLISHED
9 March 2021

Keywords: Nb_3Sn superconductors, upper critical field, critical current density, grain refinement, internal oxidation, artificial fluxon pinning

Supplementary material for this article is available online

Abstract

The inhibition of Nb_3Sn grain growth in the presence of ZrO_2 nanoparticles appears to be one of the most promising method for pushing the critical current densities of Nb_3Sn superconducting wires to levels that meet the requirements set for the Future Circular Collider. We have investigated the effect of ZrO_2 nanoparticles formed by the internal oxidation of Zr on the superconducting properties and microstructure of Nb_3Sn formed from Nb-1 wt%Zr, Nb-7.5 wt%Ta, Nb-7.5 wt%Ta-1 wt%Zr and Nb-7.5 wt%Ta-2 wt%Zr alloys. A monofilamentary wire configuration was used, with a 0.22 mm outer diameter Nb-alloy tube containing a core of powdered metal oxide (SnO_2, CuO or MoO_3) as oxygen source and successive deposits of Cu, Sn and Cu on the outer surface. As determined from inductive measurements, the layer critical current densities of the samples based on Nb alloys with internally oxidized Zr were superior to those based on Nb-7.5 wt%Ta. The samples based on Nb-7.5 wt%Ta-1 wt%Zr and Nb-7.5 wt%Ta-2 wt%Zr showed higher critical current densities at high magnetic fields (above 10–15 T), and upper critical fields exceeding 28.5 T at 4.2 K (99% normal state resistivity criterion). A record value of 29.2 T of the upper critical field at 4.2 K was obtained on samples based on Nb-7.5 wt%Ta-2 wt%Zr. Hypotheses are proposed and discussed for explaining this unexpected increase of the upper critical field, by considering the possible effects of non-oxidized Zr on the superconducting properties of Nb_3Sn and of the oxidized Zr on the formation and microchemistry of Nb_3Sn. Regardless of sample type the Nb_3Sn grains observed in our samples have an aspect ratio of 1.5–1.7. When compared in the short axis direction, the mean distance between grain boundary intercepts (lineal intercept method) is ∼40% smaller in the samples with internally oxidized Zr than in the reference samples based on Nb-7.5 wt%Ta. In the long axis direction the reduction is of 20%–30%.

1. Introduction

The generation of high magnetic fields is one of the most important applications of superconductivity, not only from the point of view of the mass of material that is used but also because of the huge impact on energy consumption and how this enables applications that would otherwise be unfeasible or prohibitive in terms of cost. The dipole and quadrupole electromagnets used to guide and focus the beams of charged particles in high-energy physics accelerators like the Large Hadron Collider (LHC) of CERN [1] constitute one such example. These applications are also the driving force for research and development in the field of applied superconductivity. New momentum was given to the research and development of Nb_3Sn superconducting wire in recent times by the high-luminosity upgrade of the LHC [2] and the study launched by CERN for a

Future Circular Collider (FCC) [3]. The critical current density (J_c) specified for Nb_3Sn in one of the FCC concepts [4] is not yet available in commercial wires [5], but recent work [6] has shown that it can be achieved. The work reported here is motivated by this need to further optimize the properties of Nb_3Sn wires in view of achieving and exceeding the requirements of the FCC study.

The development of Nb_3Sn superconductors has a long history (see for example [7]) throughout which all the features and processing conditions that can affect the current carrying capacity and its magnetic field dependence were subject to optimization. Among all the approaches used to improve the current carrying capacity of Nb_3Sn superconductor wires, the one that has gained most interest and led to remarkable progress in the last years is of increasing the number concentration of the sites on which the fluxons are pinned. This renewed interest was spurred by the major success of Xu *et al* [8, 9] of refining the grain structure of Nb_3Sn with ZrO_2 nanoparticles.

To impede grain growth and help in the nucleation of new grains, ZrO_2 precipitates were first included in Nb_3Sn tapes by researchers at the General Electric Research and Development Center [10]. A tape approach was also used by Rumaner *et al* [11] in 1994: oxygen was supplied into a Nb-Zr foil by anodization and subsequent annealing. After being coated with Cu–Sn, the foil was heat treated at 1050 °C to form Nb_3Sn with ZrO_2 precipitates. The Nb_3Sn formed had a ten times smaller grain size than the witness sample without internally oxidized ZrO_2 precipitates.

The first published attempts to include ZrO_2 in Nb_3Sn round wires come from Zeitlin *et al* [12, 13]. As pre-dissolving oxygen in Nb–Zr markedly increases its strength and thus makes the wires hard to process, Zeitlin *et al* added SnO_2 powders into the Sn core of monofilamentary internal Sn strand. The oxygen supplied by the SnO_2 was intended to diffuse into the Nb–Zr alloy and oxidize the Zr during the heat treatment applied to form Nb_3Sn. However, no grain refinement was observed in samples reacted at or below 850 °C.

The first undoubtedly successful attempt to refine Nb_3Sn grains with oxide precipitates in samples with a round wire geometry was recently achieved by Xu *et al* [8, 9]. They proceeded by fabricating a $Sn/Cu/SnO_2/Nb$-1Zr tubular composite in which the SnO_2 oxygen source (in powder form) is placed in direct contact with the Nb alloy, rather than being separated from it by a Cu layer as was the case for the design of Zeitlin *et al* [13]. When reacted at 650 °C, Nb_3Sn grain sizes more than two times smaller (43 nm compared with 91 nm) were obtained in the composite containing SnO_2 than in the reference sample. The critical current density was accordingly improved. Heat treatments performed at lower temperatures (namely 625 °C) led to even finer grains, in the range of 20–50 nm with an average of 36 nm. Moreover, the peak in the pinning force density is shifted to higher magnetic fields, to about 0.30–0.34 of the irreversibility field from the 0.2 value found in similar samples without ZrO_2. The reduction in grain size and the enhancement of the flux pinning properties were confirmed for powder-in-tube wires with Cu_5Sn_4 as the Sn source [14]. The shifts to higher magnetic fields of the maximum in pinning were attributed to a point defect pinning contribution [14] and/or individual pinning [15].

To further improve the high field transport properties, ternary additions to enhance the upper critical field of these wires with a ZrO_2-refined microstructure were the next logical step. Xu *et al* [16] undertook this study with Nb-0.6%Zr-3at%Ta [*sic*] and Nb-1%Zr-4at%Ta [*sic*] precursor alloys, Ta being the H_{c2}-enhancing dopant. It was shown that it is possible to obtain a fine-grained structure (and thus high J_c) because of the ZrO_2 and a high upper critical field because of the Ta. Further optimizations of wires based on Nb-1 wt%Zr-7.5 wt%Ta filaments have led to record high critical current densities [6]. Recently, the same group has shown that such samples have upper critical fields that are about 1 T higher than those of state of the art powder in tube Nb_3Sn wires [17].

Hafnium, a highly reactive transition metal in group four of the periodic table, like Ti and Zr, is another candidate alloying element for being internally oxidized to form inclusions capable of inhibiting the coarsening of Nb_3Sn grains. It was first investigated by Balachandran *et al* [18] in monofilamentary wires based on Nb-4at%Ta-1at%Hf. In the presence of SnO_2 as an oxygen source the addition of Hf led to the expected grain size refinement and critical current density increase, to values better than those of a similar wire based on Nb-4at%Ta-1at%Zr. What was not expected was the achievement of even higher critical current densities and comparable grain sizes (albeit with a slightly larger average of 68 nm as compared with 55 nm) for a wire of the same configuration but without SnO_2 [18]. This surprising result was attributed to the small grain size of the Nb-4at%Ta-1at%Hf filament material and its lack of recrystallization during the reaction heat treatment to form Nb_3Sn, maintaining a dense structure of grain boundaries suitable for the faster diffusion of Sn and thus enhanced nucleation of Nb_3Sn.

This work summarizes the results of a project aimed at studying and optimizing the use of internal oxidation of Zr to improve the superconducting properties of Nb_3Sn. We explored several types of oxygen source and looked at the effect of the addition of Ta to Nb_3Sn with internally oxidized Zr. A remarkable

Table 1. Summary of wire configurations. All alloy fractions are given as weight (mass) percentages (per total mass of alloy).

Filament material (wt%)	Metal powder used as oxygen source	Particle size range of powder used as oxygen source (nm)	Diameters of rod and hole for powder (mm)	Nominal Cu/Sn volume ratio	Nominal Nb/Sn volume ratio
Nb-1Zr	SnO_2	35–55	12.0/2.5	0.42	1.6
Nb-1Zr	MoO_3	13–80	12.0/2.5	0.42	1.6
Nb-1Zr	CuO	<80	12.0/3.4	0.42	1.6
Nb-7.5Ta-1Zr	SnO_2	35–55	12.1/2.5	1.3	2.1
Nb-7.5Ta-2Zr	SnO_2	35–55	12.1/3.4	1.3	2.0
Nb-7.5Ta	MoO_3	13–80	11.6/2.5	0.42	1.6
Nb-7.5Ta	—	—	11.6/–	0.42	1.7
Nb	MoO_3	13–80	11.8/2.5	0.42	1.6

finding is that the upper critical field is higher in samples based on Nb–Ta–Zr alloys than in samples based on Nb-7.5Ta, thus suggesting the potential for further property improvements at high magnetic fields. The possible mechanisms by which the presence of Zr and/or O can lead to this enhancement of the upper critical field are analyzed by taking into account our own experimental observations and other publications on the influence of additional elements and the diffusion kinetics on the upper critical field of Nb_3Sn.

2. Experimental methods and details

2.1. Sample configurations and preparation

The monofilamentary Nb_3Sn samples presented here have an external Sn configuration, in which a Nb alloy filament 0.22 mm in diameter is surrounded by successive electrodeposited layers of Cu, Sn and Cu. In the center of the Nb alloy, a compacted core of metal oxide powder serves as the oxygen source for the internal oxidation of Zr. Already used (without the outer Cu deposit) in early Nb_3Sn development efforts [19], this design was chosen because of the ease with which the Cu/Sn and Nb/Sn ratios could be adjusted.

Multiple combinations of different Nb alloys and oxygen sources were studied, in an attempt to further improve the high magnetic field properties and identify materials that may be of interest for the development of multifilamentary wire. The wires configurations studied are summarized in table 1.

The Nb alloy filament was obtained by the swaging and cold wire drawing (without intermediate annealing) of an annealed (in the case of the Zr containing alloys) or cold worked (in the case of the Nb-7.5 wt%Ta alloy) round bar of 11.6–12.0 mm diameter with a central hole filled with oxide powder at tap density. For each oxide type, the holes were sized to accept enough oxide to provide the oxygen necessary for oxidizing all the Zr atoms in the Nb alloy, at a 50% packing density of the oxide powder. A notable exception is that of the wire based on Nb-1Zr filament material with CuO as the oxygen source, in which the diameter of the hole was inadvertently larger than needed, corresponding to 3.6 oxygen atoms for each zirconium atom instead of 2. For the Nb alloys that do not contain Zr, the hole was sized as for an alloy containing 1 wt% Zr. All the nano-sized oxide powders were purchased from US Research Nanomaterials Inc. and had purities exceeding 99%.

The inner Cu layers were electro-deposited from an oxygen-free electronic grade Cu wire anode by using the Slotocoup Cu 50 process from Dr.-Ing. Max Schlötter GmbH & Co. KG of Geislingen/Steige, Germany. A 99.95% Sn bar from Alfa Aesar was used as the anode for Sn deposition, the process being Slototin 40 from Dr.-Ing. Max Schlötter GmbH. These depositions were performed on multiple 10 cm long wire segments for each configuration.

2.2. Heat treatments

The as-deposited wire samples were heat treated at 650 °C for 200 h, either in vacuum or enclosed in quartz tubes under 800 mbar of Ar gas.

2.3. Superconducting property measurements

Temperature and magnetic field dependent measurements of the magnetization (M) were performed in a SQUID magnetometer on samples of 3–5 mm in length that were extracted from different positions of each heat treated wire segment. Superconducting transition temperatures (T_c) were determined from the magnetic moment vs temperature (T) curves recorded in a magnetic field (B) of 2 mT oriented along the axis of the cylindrical samples. T_c values were defined as the temperatures at which a percentage of 99%, 90%, 50%, 10% and 1% of the magnetic moment of the fully superconducting Nb_3Sn that is yet to be added to

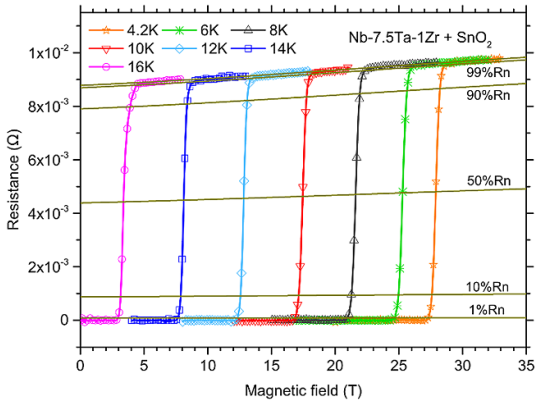

Figure 1. Dependence of the resistance on the magnetic field at various temperatures for a sample based on Nb-7.5 wt%Ta-1 wt%Zr with SnO_2 as oxygen source. R_n is the normal state resistance, determined just above the transition on a linear fit of its dependence on the magnetic field.

reach the full exclusion of the magnetic field. The Nb_3Sn transition was considered finished (i.e. 0% of the full magnetic moment yet to be added) just before the onset of the superconductivity of the Nb alloy.

The dependence of the critical current density (J_c) on the magnetic field was calculated from *M(B)* loops recorded in magnetic fields up to 7 T. We used the critical state model of Bean [20] as extended by Kim *et al* [21, 22] and applied to a hollow cylinder geometry [23] in transverse orientation with respect to the magnetic field.

$$J_c = \frac{30\pi}{4} \times \frac{1}{1-\left(\frac{d}{D}\right)^3} \times \frac{\Delta M}{D}.$$

J_c is the critical current density (in A cm^{-2}) of the superconductor layer.
d and D are the inner and outer diameters (in cm) of the superconductor in the shape of a hollow cylinder.
ΔM is the opening (in emu cm^{-3}) of the *M(B)* loop at the magnetic field of interest.

The inner (d) and outer (D) diameters of the superconductor layer were determined from electron microscopy images taken on polished and/or fractured cross-sections of the superconductor samples, at the boundaries between the fine-grained Nb_3Sn area and the unreacted Nb alloy, and between the fine-grained and coarse-grained Nb_3Sn areas, respectively. As these boundaries are not perfectly circular, in each case an average diameter was determined from the area encompassed by the boundary by calculating the diameter of the circular disk that has the same area. To this first deviation from the hollow cylinder model, we have to add the variation of d and D along the length of the samples, as well as possible intrinsic variations of the actual J_c values. These factors have led to evident sample-to-sample variability for the four J_c samples measured for each configuration. For better readability, we have selected for the graphs presented here only the two of the four samples that were closest to each other and to the average of the four.

The pinning forces densities (F_p) were calculated as the product of the critical current density (determined as above) and the corresponding magnetic field: $F_p = J_c \times B$.

Transport measurements of the critical current densities were not possible because of significant redistribution of the Cu during the reaction heat treatment (as will be shown later) combined with the formation of a thin but highly adherent layer of oxide at the surface of the samples.

For selected samples, we have determined the upper critical field as a function of temperature from low current transport measurements in magnetic fields of up to 33 T at the European High Magnetic Field Laboratory in Grenoble, France. Because of dimensional constraints, these samples were not exactly the same as those measured in the SQUID magnetometer, but they were of the same type, extracted from the same or a similar batch. During these measurements, the resistance of 7–10 mm long samples oriented transversally with respect to the applied magnetic field was measured using a four-point method, with current densities in the superconductor in the range of 0.1–0.2 A mm^{-2}. The upper critical fields were defined as the magnetic fields at which the lines corresponding to the superconducting transition cross the respective criterion line, for resistive criteria of 1%, 10%, 50%, 90% and 99% of the normal state resistance (R_n), as shown in figure 1. In the absence of a high electrical conductivity Cu stabilizer, the probe voltages we measured were higher and thus significantly less affected by noise than similar measurements reported in other papers [16, 24], which allowed straightforward determinations even at the 99% and 1% criteria.

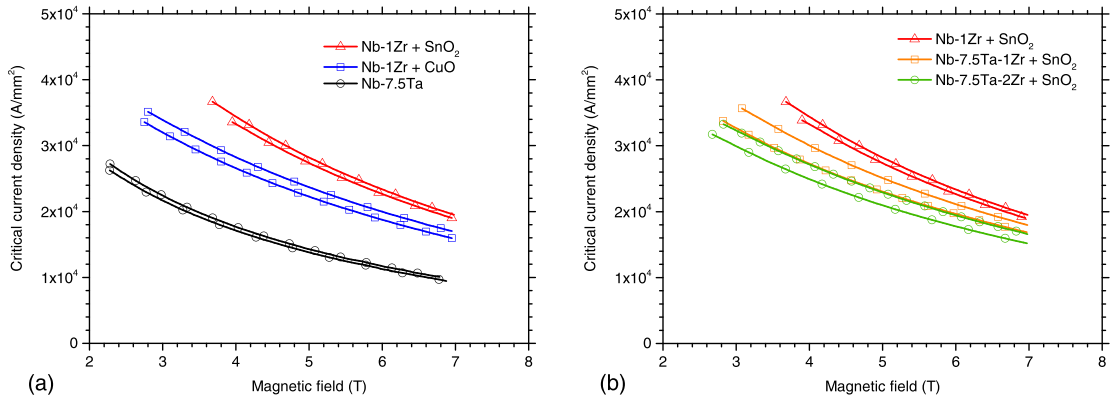

Figure 2. Critical current densities (at 4.2 K) of (a) samples based on Nb-1Zr with an oxygen source compared with samples based on Nb-7.5Ta without an oxygen source, and (b) of samples based on Nb–Ta–Zr with an oxygen source compared with samples based on Nb-1Zr. Values determined from magnetization measurements.

The uncertainty intervals reported for the superconducting transition temperatures and the upper critical fields were determined from the sample-to-sample variation as being half the width of the interval between the lowest and the highest determined value in a set of 2–4 samples of the same type, the measurement uncertainty being considered negligible by comparison.

2.4. Microstructure analysis

Polished and/or fractured transverse sections of the wire samples were analyzed by scanning electron microscopy to determine the inner and outer diameter of the fine-grained superconducting Nb_3Sn layers.

The reported grain size distributions are based on the distances between grain-boundary intercepts using a lineal intercept approach on images of transverse fracture surfaces obtained by field emission scanning electron microscopy. The grains often showed an elongated shape: to obtain the size distribution in both directions, lines were drawn in the direction of the long axis of the grains as well as the perpendicular direction. The initial visual evaluation of the fractured surfaces did not reveal a clear difference between the fine Nb_3Sn grains close to the periphery and those close to the interface with the unreacted Nb alloy, so the areas whose images were included in the grain size analysis were randomly selected across the layer and multiple samples of the same configuration.

3. Experimental results

3.1. Superconducting properties

The first sample series we prepared and tested did not include samples based on ternary Nb–Ta–Zr alloys. This initial study was aimed at confirming the effect of the internal oxidation of Zr on the superconducting properties and microstructure of Nb_3Sn and to evaluate different oxygen sources. Based on these critical current density determinations, our samples did not show a positive effect of MoO_3 as an oxygen source in Nb-1Zr, the values obtained being comparable with those obtained on the reference wires without Zr.

When used as an oxygen source for the internal oxidation of Zr in samples based on Nb-1Zr, CuO was found to lead to critical current densities slightly lower than those of similar samples having SnO_2 as oxygen source, as seen in figure 2. However, given the relatively large sample-to-sample variability, it cannot be excluded that in other wires, especially at high magnetic fields, the CuO oxygen source might lead to critical current densities comparable with those of wires having SnO_2 as oxygen source.

Additional sample series were prepared for checking the effect of Ta addition to the Nb-1Zr alloy on the superconducting properties of the resulting Nb_3Sn. As shown in figure 2(b), at magnetic fields below 7 T the critical current densities of our samples based on Nb–Ta–Zr alloys were lower than those of the samples based on Nb-1Zr. However, the field dependence strongly suggests that at magnetic fields higher than 10–15 T the critical current densities of Ta-containing samples will surpass those of the samples based on Nb-1Zr because of higher irreversibility fields. Even though valid for the samples we have prepared and measured, at the moment we cannot draw a definite and general conclusion regarding the superiority in critical current density of the Nb-7.5Ta-1Zr samples over Nb-7.5Ta-2Zr samples, because of the sample-to-sample variability, both between samples of the same wire segment and from wire segment to wire segment of the same configuration.

Table 2. Magnetic fields and normalized magnetic fields at which the pinning force density reaches its maximum. The reported values were calculated as arithmetic means of the values determined on three to four samples.

Wire configuration	$B(F_{pmax})$ at $T = 4.2$ K (T)	$b(F_{pmax}) = \frac{B(F_{pmax})}{B_{c2}(10\%\,R_n)}$
Nb-7.5Ta-1Zr + SnO_2	6.1	0.21
Nb-7.5Ta-2Zr + SnO_2	5.9	0.22
Nb-7.5Ta	5.2	0.19
Nb-1Zr + SnO_2	5.3	0.20
Nb-1Zr + CuO	5.8	0.24

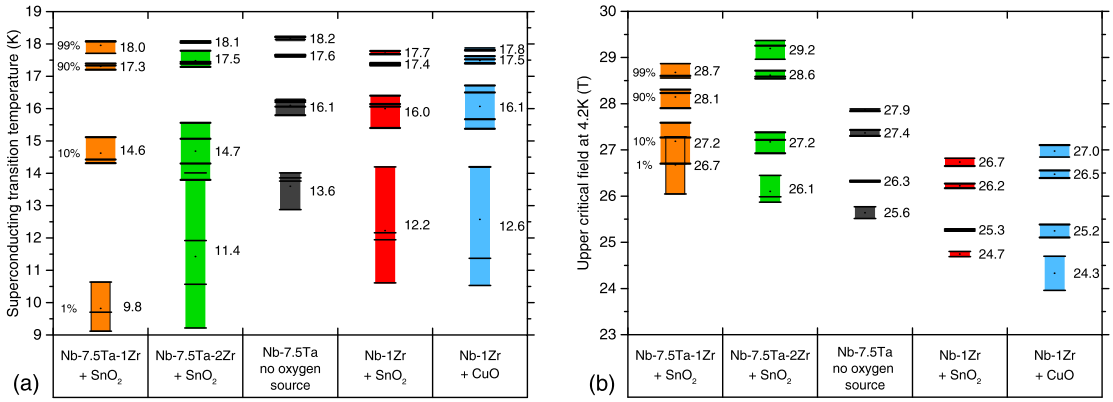

Figure 3. (a) Superconducting transition temperatures obtained from magnetic measurements, and (b) upper critical fields obtained from transport measurements at 4.2 K. For each criterion (99%, 90%, 10%, 1% from top to bottom) and sample type, the floating column indicates the range of the experimentally determined values for the respective criterion. The black horizontal lines correspond to the actual measured values whereas the numerical value shown to the right of the column is the mean value (of the values determined on two to four samples). The mean values and their uncertainties are tabulated in the supplemental material (tables of superconducting properties and additional plots of the normalized pinning force density available online at stacks.iop.org/JPMATER/4/025003/mmedia).

Table 2 refers to the following physical quantities that characterize the magnetic field dependence of the fluxon pinning in our samples:

F_{pmax} is the maximal value of the pinning force density;
$B(F_{pmax})$ is the magnetic field at which the pinning force density reaches its maximal value;
$b(F_{pmax})$ is the normalized magnetic field at which the pinning force density reaches its maximal value, relative to the upper critical field B_{c2} determined with a criterion of 10% of the normal state resistance (value that was found to lead to the best scaling of the normalized F_{pmax} on these samples).

The upper critical field results obtained from resistive measurements (values at 4.2 K are summarized in figure 3(b)) confirm that the samples based on filament materials containing Ta have higher upper critical fields than those based on Nb-1Zr, at all the temperatures investigated. What is most important to note here is that our samples based on Nb–Ta–Zr alloys have upper critical fields that are higher than those of the samples based on Nb-7.5Ta. These results will be further discussed in the analysis section of this paper.

To obtain information regarding the fluxon pinning in our samples, we have prepared graphical representations of the pinning force density normalized to its maximal value as a function of the magnetic field normalized to each of the types of critical fields that we have determined (figure 3(b)), from J_c values obtained at the temperatures of 4.2, 6.0, 8.0, 10.0, 12.0, 14.0 and 16.0 K.

Based on visual evaluations of the graphical representations in the range of normalized magnetic fields of 0.2–0.3, the best scaling of the normalized flux pinning force was found when the normalizing field was the critical field obtained with a criterion of 10% of the normal state resistance, a typical example being shown in figure 4 for a sample based on Nb-7.5Ta-1Zr (see supplemental material for other examples). The 16.0 K curve shows a lack of overlap with the other curves, evident mostly at high normalized magnetic field. As will be discussed later, this may be related to the inhomogeneity of the Nb_3Sn layer. With the notable exception of the curve of the sample based on Nb-1Zr + CuO, which shows a maximum at a reduced field of 0.24, the other curves have their maxima at normalized magnetic fields of 0.19–0.22 (table 2).

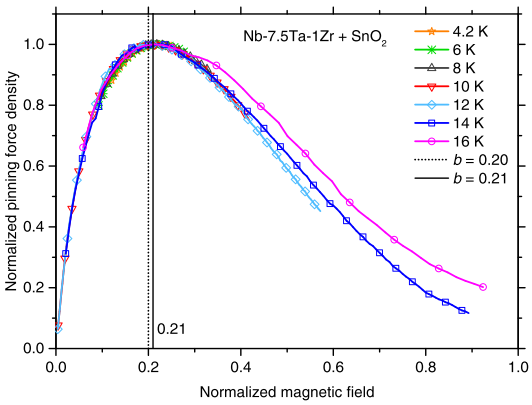

Figure 4. Normalized flux pinning force density as a function of the normalized magnetic field b, for a sample based on Nb-7.5Ta-1Zr with SnO_2 as oxygen source. The magnetic field was normalized to the upper critical field determined with a criterion of 10% of the normal state resistivity.

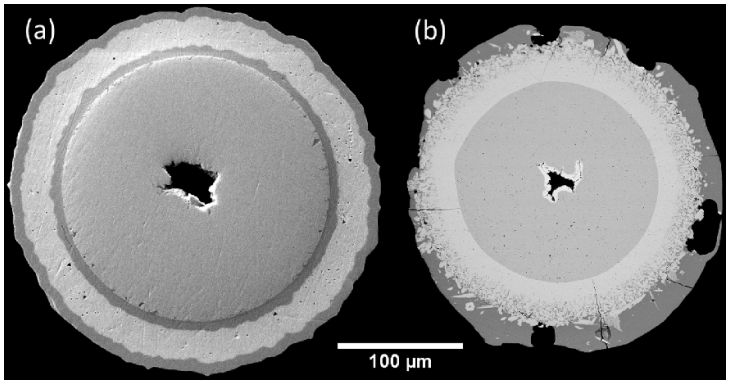

Figure 5. Typical cross-sections of (a) a precursor wire sample and (b) a sample after undergoing a reaction heat treatment at 650 °C for 200 h to form Nb_3Sn. Images taken by scanning electron microscopy on polished transverse sections.

3.2. Microstructural observations

As mentioned earlier, during the reaction heat treatment the successive Cu/Sn/Cu layers on the surface of the Nb alloy of the precursor wire (cross-section in figure 5(a)) intermix entirely, which leads eventually to a severe redistribution of the Cu. An example can be seen in the cross-section of figure 5(b). Based on the amount of Sn initially supplied, of Nb_3Sn formed and Sn left in the Cu at the end of the heat treatment, we estimate that some of the Sn initially present in the wire was lost by evaporation during the reaction heat treatment.

The Sn/Cu ratio and the two-layered structure of the Nb_3Sn indicate that the superconductor forms by a sequence similar to the one of other wires with a high Sn/Cu ratio (powder-in-tube [25–27], tube-type [28, 29] or some Sn-rich rod-type wires [30, 31]). In such wires, as the heat treatment progresses, Sn reacts with the Nb to form $NbSn_2$ followed by Nb_6Sn_5; then, as the Sn supply diminishes and Sn diffuses farther into unreacted Nb, this Nb_6Sn_5 transforms into coarse-grained Nb_3Sn, and new fine-grained Nb_3Sn forms from Nb and incoming Sn. In our wires, the coarse-grained Nb_3Sn is visible at the outer periphery (figure 5(b)), with a large number of Cu–Sn inclusions, and is followed towards the center of the wire by a continuous and homogeneous layer of fine-grained Nb_3Sn (figure 5(b)) that is 15–30 μm thick, depending on the sample. The relatively large sample-to-sample scatter of the amount of coarse and fine-grained Nb_3Sn, most probably due to non-reproducible Cu redistribution and Sn loss, does not allow us to draw any conclusion regarding the reaction kinetics as a function of Nb alloy and oxygen source.

Our attempts to closely examine the Sn content in Nb_3Sn and its variation across the layer by Energy dispersion x-ray spectroscopy (EDS) were not successful because the Zr was not detected, its Lα peak being completely overlapped by a very prominent Lα peak of Nb. Moreover, the Ta concentration determined by standardless quantification on its Mα peak was not accurate. In the tests we performed, the pure-element standardized wavelength dispersion x-ray spectroscopy quantifications did not give accurate values of the Zr content in the Nb–Ta–Zr alloys. Further experiments and different standardization procedures will surely

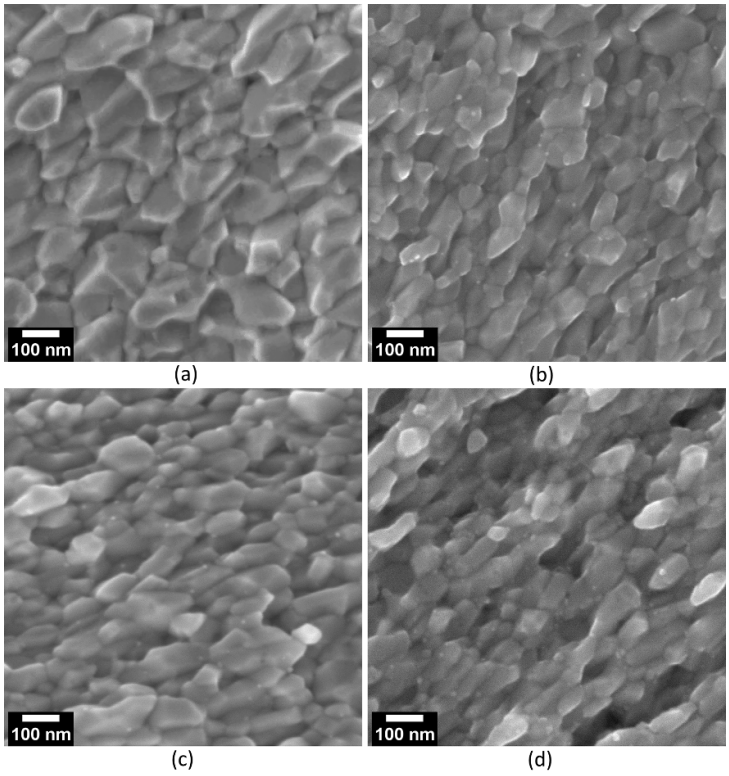

Figure 6. SEM images of Nb_3Sn grains at fractured surfaces from samples based on (a) Nb-7.5Ta, (b) Nb-1Zr + SnO_2, (c) Nb-7.5Ta-1Zr + SnO_2 and (d) Nb-7.5Ta-2Zr + SnO_2.

lead to accurate results but they are still to be performed and thus not available at this time. We have checked by EDS the variation of the Sn content from the periphery of the reaction layer (Sn source side) to the interface with the unreacted Nb alloy and obtained a value of around 1–1.5 at% on multiple wire configurations. The measurement points were a few microns away from the actual interfaces, to take into account the beam interaction volumes.

At the center of the unreacted Nb alloy is the remainder of the oxygen source. In the wires where SnO_2 was the oxygen source, the hole that contained the oxide is surrounded by a $NbSn_2$ layer (figure 5(b)) formed by the reaction of Nb with the elemental Sn released by the reduction of the oxide during the reaction heat treatment. In the wires having CuO as oxygen source, metallic Cu was observed at the end of the heat treatment in the hole that previously contained CuO. These observations confirm the reduction of the oxide during the reaction heat treatment.

The electron microscopy images of Nb_3Sn fracture surfaces show a clear refinement of the grains in the samples based on Nb–Zr and Nb–Ta–Zr alloys and an oxygen source (figures 6(b) and (d)) as compared with samples based on Nb-7.5Ta alloy without added oxygen (figure 6(a)).

Nanoparticles, identified in previous work [8] as being ZrO_2, were detected in a large number of such high resolution images of samples based on Nb–Zr and Nb–Ta–Zr alloys, see for example figures 6(b) and (d). Given the image to image variations we have not attempted to quantify their number concentration or volume fraction, nor to closely look at the variation of these quantities with the position. It is clear however that their number concentration is not uniform throughout the samples. For this reason the differences in ZrO_2 nanoparticle concentration that may be inferred from the images (b) and (d) of figure 6 should not be considered representative.

As revealed by the imaged fracture surfaces, the Nb_3Sn grains are not equiaxed but slightly elongated, with an aspect ratio of 1.5–1.7. There seems to be no relationship between the orientation of the long axis of these grains and the radial direction in the wires, the direction of Nb_3Sn growth. Measures of the Nb_3Sn grain size in these materials, the mean and median values of the distance between grain boundary intercepts in the lineal intercept method (table 3), confirm the visual evaluation: the grains are substantially smaller in samples based on internally oxidized Nb–Zr alloys than in the samples based on Nb-7.5Ta without added oxygen. This is valid for both the long axis and the short axis of the grains. However, the refinement appears slightly more pronounced in the short axis direction, with a ratio of around 0.6 between the respective lengths in the internally oxidized and the Nb-7.5Ta-based samples as compared to 0.7–0.8 in the long axis direction.

Table 3. The mean, median and standard deviation of the distribution of distances between grain boundary intercepts in the lineal intercept method used to evaluate the grain size distribution in Nb_3Sn. Results are given both in the direction of the long axis and of the short axis of the grains.

Wire configuration	Mean, long axis direction (nm)	Median, long axis direction (nm)	Std. dev., long axis direction (nm)	Mean, short axis direction (nm)	Median, short axis direction (nm)	Std. dev., short axis direction (nm)
Nb-7.5Ta-1Zr + SnO_2	87	82	38	60	55	25
Nb-7.5Ta-2Zr + SnO_2	95	85	48	55	51	23
Nb-7.5Ta	118	108	56	92	85	45
Nb-1Zr + SnO_2	95	86	48	57	53	26
Nb-1Zr + CuO	90	81	46	51	47	24

4. Analysis of results

The critical current densities follow the trend expected based on the previous work of Xu *et al* [9]: they increase at all fields when Zr and an oxygen source for the internal oxidation of the Zr are added to the binary Nb-based Nb_3Sn. In our monofilamentary wires we have found that the presence of Ta in Nb_3Sn with internally oxidized Zr improves the critical current densities at high magnetic fields (in excess of roughly 10 T at 4.2 K) whereas at low fields the samples without Ta remain superior. We confirm thus the findings of Xu *et al* [16] who showed for the first time that the addition of Ta to Nb_3Sn with internally oxidized Zr vastly improves the critical current densities at high magnetic fields. The absolute values of the critical current densities will not be compared and discussed here, as our experimental monofilamentary wires are far from being optimized and show a significant sample-to-sample variability.

According to the summary in table 2, the calculated flux pinning forces of our samples show a maximum at magnetic fields very close to $0.2 \cdot B_{c2}$(10% Rn), which is indicative of the normal surface pin geometry [32]. On their samples, Xu *et al* [8, 9] found that in many cases this maximum shifts towards 0.33 of the normalized magnetic field, and even 0.4 [15] for samples reacted at lower temperatures (thus even lower grain sizes). These shifts were attributed to additional fluxon pinning mechanisms [15]. We think that the density of ZrO_2 nanoparticles in our samples is lower than in the samples of Xu *et al* This hypothesis would be supported by the observation that our SEM micrographs of fracture surfaces do not show the same ubiquitous presence of ZrO_2 nanoparticles, but would also imply a radial gradient of the grain sizes (caused by a diffusion-limited supply of oxygen from the center towards the periphery of the wire), which we have not visually observed. A study of the ZrO_2 concentration and/or grain size as a function of the radial position would be needed to answer this question. What is clear is that the oxygen supply is not generous in our wires: it was calculated for oxidizing all the Zr but without an excess to drive the kinetics in the later stages. In view of this observation, it is not surprising that the sample series that had (inadvertently) a slightly oversized oxygen source has a peak pinning force density at a higher normalized magnetic field of 0.24.

Based on the curves of the normalized pinning force as a function of the normalized magnetic field (example in figure 4), the temperature scaling of the flux pinning density dependence on the magnetic field between 4.2 K and 15 K is respected. As evident in figure 4, at temperatures of 16 K (and sometimes, to a lesser extent at 15 K) a field dependence of a different shape and irreversibility limit emerges. It appears that the part of Nb_3Sn that has the highest upper critical fields and superconducting transition temperatures has a different pinning behavior than the rest.

Based on our analysis of the distribution of the distances between grain boundaries in the lineal intercept method, the reduction in Nb_3Sn grain size is similar for samples based on Nb–Ta–Zr and Nb-1 wt%Zr alloys. The mean and median sizes we determined cannot be directly compared with the 'average grain sizes' reported by Xu *et al* [8, 9, 16] or Balanchandran *et al* [18] as the grains are not equiaxed, and defining a mean or median grain size in such a case is not straightforward. These issues will be discussed elsewhere [33]. However, an area- or volume-averaged grain size would most probably fall in the 50–100 nm range for our internally oxidized samples, definitely finer than the 100–150 nm range encountered in conventional wires.

The onset (99% criterion) superconducting transition temperatures of figure 3(a) confirm the known increase of the T_c of Nb_3Sn when small amounts of Ta are present [34]. The addition of 1 wt% Zr to the Nb precursor of the binary Nb_3Sn, and 1–2 wt% Zr to the Nb-7.5Ta precursor of the Ta-doped Nb_3Sn, has little effect on the onset T_c of Nb_3Sn, which is consistent with previous reports [34]: the maximum reduction is 0.2 K. As the T_c-s obtained with a 1% criterion show very large scatter (figure 3(a)) it is better to use the 10% values to measure the widths of the transitions.

Table 4. Various measures of the widths of the superconducting transitions in varying magnetic fields at 4.2 K.

Sample	B_{c2} (99% R_n) − B_{c2} (1% R_n) (T)	B_{c2} (99% R_n) − B_{c2} (50% R_n) (T)	B_{c2} (90% R_n) − B_{c2} (10% R_n) (T)
Nb-7.5Ta-1Zr + SnO_2	2.0 ± 0.6	1.0 ± 0.3	1.5 ± 0.3
Nb-7.5Ta-2Zr + SnO_2	3.1 ± 0.5	1.2 ± 0.3	1.4 ± 0.3
Nb-7.5Ta	2.2 ± 0.2	1.0 ± 0.1	1.0 ± 0.1
Nb-1Zr + SnO_2	2.0 ± 0.1	1.0 ± 0.1	1.0 ± 0.1
Nb-1Zr + CuO	2.6 ± 0.5	1.0 ± 0.1	1.2 ± 0.2

Based on the difference between the 99% and the 10% T_c values, the widths of the transitions in the samples based on Nb–Ta–Zr are about 1 K wider than those of the samples based on Nb-7.5Ta and Nb-1Zr, which may suggest that the Sn concentration gradient is different and/or that the Ta and Zr are not as uniformly distributed in our ternary Nb–Ta–Zr alloys. Despite the larger thicknesses of the fine-grained regions in our samples (15–30 μm in our samples in comparison to ∼10 μm), the transition widths are comparable with those measured by Tarantini *et al* [35] and Baumgartner *et al* [36] on powder-in-tube wires based on Nb-7.5Ta. This suggests that the differences in T_c (and thus of the differences in Sn content) between the best and the poorest Nb_3Sn regions of our samples are comparable with those encountered in the practical, industrial wires studied in these papers. In such industrial powder-in-tube Nb_3Sn wires that are heat treated for optimal critical current densities at 12–15 T, the gradient in Sn concentration is of about 0.1 at%Sn μm^{-1} (see for example [36] and references therein). Based on this and on the 15–30 μm thickness of the fine-grained regions, we would expect that in our samples the Sn content varies by 1.5–3 at% from the regions that are richer to those that are poorer in Sn.

There seems to be no obvious relationship between the overall width of the transition, as measured by the difference between B_{c2}(99%) and B_{c2}(1%) in table 4, and the filament alloy. However, comparing the critical field intervals between consecutive criteria one can conclude that most of this transition width comes from the bottom half of the transition, the one that corresponds to lower magnetic fields. The upper half of the transition, between 50% and 99% of the normal state resistivity, shows a fairly constant width of 1.0–1.2 T (table 4) which indicates that the best half has about the same composition gradient in all the sample types and that the corresponding critical magnetic fields are more suitable for comparison between different filament materials and with industrial wires.

At the same criterion of 50%, the upper critical fields of 26.9 ± 0.1 T at 4.2 K of our samples based on Nb-7.5 wt%Ta are practically equal to those measured by Suenaga *et al* [34] on monofilamentary bronze route wires based on Nb-7 wt%Ta in the absence of the strain induced by the bronze matrix.

More recently, Godeke *et al* [24] measured 26.4–26.9 T at 4.2 K (99% criterion) on commercial Ta-doped Nb_3Sn bronze route and powder-in-tube multifilamentary wires reacted at 675 °C or below, values that are 1.1–1.5 T lower than our 27.9 T, the larger difference being with the bronze route wires. As the comparison is being made on the best part of the material, there is no need to take into account the width of the transition in this case. This is not the case for the comparison with the results of Nazareth *et al* [28], who measured 26.9–27.1 T at 4.2 K (90% criterion) on their best samples of Ta-doped Nb_3Sn tube-type multifilamentary wires reacted at 675 °C, with a transition width of 0.6–0.8 T between the 10% and 90% criteria. Given that this transition width is lower than the 1.4–1.5 T found in our samples (table 4), the 90% criterion may not be probing at the same deviation from the best material, which means that the difference of 0.3–0.5 T in critical field may be slightly larger when evaluated for the best material, at the 99% criterion. We believe that these differences between some of the published data and our results on Ta-doped Nb_3Sn can be explained by a lower axial pre-compression on our monofilamentary samples as compared to the stabilized multifilamentary commercial wires. It is well known that the strain, externally applied or due to the differential thermal contraction of the different wire constituents, has a notable effect on the superconducting properties (see for example [37]). Based on the results of Ten Haken *et al* [38] and Godeke *et al* [39] we can estimate that in the compressive range the Kramer extrapolated irreversibility field (and therefore the upper critical field) of Ta-doped Nb_3Sn can change by as much 0.7–1.4 T when the absolute value of the axial strain changes by 0.1%. Bronze route Nb_3Sn wires usually have an axial precompression of 0.2%–0.5% [40–42], whereas optimized powder-in-tube wires have lower axial precompressions of ∼0.02%–0.3% [43–45]. On tube-type wires with configurations similar to those of Nazareth *et al* [28], the axial precompression was measured by Peng *et al* [46] to be of 0.35%–0.42%. Given these large variations between and within types of wire, a difference of 0.1% in axial precompression can easily be present and thus account for most if not all the difference in upper critical field between our samples and those of Godeke *et al* [24], Nazareth *et al* [28].

Based on the comparison and arguments brought above we consider that the upper critical fields obtained on our samples (in particular those evaluated with the 99% and 90% criteria) are representative of what is to be expected from these alloys as filament material in practical multifilamentary wires, provided that a degradation due to strain is taken into account.

A very important contribution of this work is that it shows convincingly that Nb_3Sn based on the Nb-7.5Ta-1Zr and Nb-7.5Ta-2Zr alloys have upper critical fields that are significantly higher than those based on Nb-7.5Ta, an alloy that otherwise was optimized as a filament material leading to a high upper critical field. Xu *et al* [16] have already shown an 1.8 T improvement of the upper critical field at 4.2 K (90% criterion) of their Ta-doped Nb_3Sn tube type wires with internally oxidized Zr over the 25.8 T measured on a RRP type Ta-doped Nb_3Sn wire (from Oxford Superconducting Technology, fabricated by their Restacked Rod Process), but neither of these values was sufficiently high to suggest the benefit of the combination of internal oxidation and Ta doping. Recent results of the same group, published during the preparation of this paper are remarkable for multifilamentary wires, showing 28.2 T at 4.2 K for a 99% criterion [17], an improvement of ∼1 T over state of the art powder in tube Nb_3Sn wires.

To our best knowledge, the upper critical fields we determined on these samples are the highest ever measured at 4.2 K (rather than extrapolated from higher temperatures) on doped Nb_3Sn, with the exception of those doped with Ga [47, 48] or Tl [47]. As is evident from figure 3(b) this superiority of the upper critical field of the samples based on Nb–Ta–Zr over those based on Nb–Ta is valid at all criteria, the highest values being obtained for the samples based on Nb-7.5 wt%Ta-2 wt%Zr. The gain of 1.2 T in upper critical field at the 90% criterion for this alloy may be of practical importance, as it has the potential of leading to improvements in the transport properties at high magnetic fields.

When considering high-field transport properties, we should probably talk more about the irreversibility field, the field at which the critical current density goes to zero. The irreversibility field is linked to the upper critical field, but its interpretation and exact relationship to the upper critical field depends on whether we consider homogeneous superconductors [49, 50] or practical superconductors with composition gradients [51]. When not directly determined from the magnetization loops at the magnetic field where the loop closes, the irreversibility field is determined from the extrapolation to zero critical current density of a plot based on the scaling law of Kramer [52]. Experiments [53, 54] and simulations [51] have shown that the irreversibility field of Nb_3Sn wires depends on the Sn composition gradient and as such it will be affected by the heat treatment temperature and duration. We can therefore expect that wires based on Nb–Ta–Zr with better designs than those of this study will have an improved Sn composition profile and therefore an irreversibility field that will approach the upper critical field. As our SQUID measurements are limited to a magnetic field of 7 T we can only make reliable Kramer extrapolations at the highest temperatures, and thus the closest indication of the irreversibility field of our samples is the upper critical field obtained with a criterion of 10%. As discussed earlier, these values led to very good scaling over the entire range of normalized magnetic fields. It is actually common to use the 10% criterion (or sometimes the 1%) as a value that is representative of the irreversibility field. Based on such an estimation, Xu *et al* [16] obtained an irreversibility fields of 26.8 T in a wire based on a Nb-7.5 wt%Ta-1 wt%Zr, 0.9 T higher than a wire based on Nb–Ta. In similar samples they have also performed Kramer extrapolations that indicated 26.3–26.6 T [17], at 0.6–0.8 T below the $B_{c2}(99\%)$. Our Nb–Ta–Zr based samples show a $B_{c2}(10\%)$ with a mean value of 27.2 T (with the best at 27.6 T), at ∼1.4 T below the $B_{c2}(90\%)$ upper critical field, and ∼2 T below $B_{c2}(99\%)$. As discussed earlier in this paper, part of the difference between our results and those of Xu *et al* [16, 17] may come from differences in axial precompression but another part may be eventually attributed to the higher Zr content in our best samples. In addition, given the larger difference from the upper critical field in our samples, there is a potential for further increase that is to be explored.

What is intriguing in this augmentation of the upper critical field of the samples based on Nb–Ta–Zr alloys is that, in the situation of full oxidation of the Zr, there should be little or no effect on the electronic properties of the normal state of the superconductor (and thus on the upper critical field), as all the Zr ends up locked in the ZrO_2 nanoparticles. In addition, the alloy having 2 wt% Zr has higher critical fields than the one with 1 wt% Zr and, as will be discussed below, Zr is not among the elements known to have an important effect on these critical fields. This leads us to make two hypotheses:

(a) Some of the Zr is left in elemental form (without being oxidized) and relatively homogeneously distributed in Nb_3Sn such that it can contribute together with the Ta to increasing the upper critical field. The manner in which this happens is still to be understood: it could be related to the site occupancy of these elements in the Nb_3Sn unit cell and/or to different effects on the normal state resistivity and the density of states.
(b) The presence of Zr and/or O affects the diffusion of Sn, which allows the formation of Nb_3Sn with a higher Sn content and thus higher upper critical field.

We will not be able to fully verify these hypotheses in this paper, but we explore the evidence for them below. The first hypothesis would be supported by our earlier argument that some of the Zr in our samples is not oxidized, but an initial verification would require a determination of the Zr content in individual grains and/or the quantitative analysis of the oxidation state of Zr. Previous work has shown that the presence of Zr by itself [34, 55] has little effect on the upper critical field of Nb_3Sn. Our own results in figure 3(b) show that there is little difference between the upper critical fields we measured at 4.2 K (90% criterion) on samples based on Nb-1Zr (26.2–26.5 $\pm$ 0.1 T) and the best binary Nb_3Sn samples [22] (26.0–26.6 T). However, it has been reported recently that simultaneous additions of Zr and Mo [56] lead to upper critical fields and critical current densities that are superior to those obtained by the addition of only one of the two elements. No explanation is given for this effect, but in our opinion the same two hypotheses can be raised.

With respect to the second hypothesis, previous reports [34, 57] show that Zr enhances the diffusion of Sn during the formation of Nb_3Sn, as indicated by the rate of formation of Nb_3Sn. But the situation is different in composites with internally oxidized Zr, where a slower growth of Nb_3Sn was observed in the usual range of reaction temperatures of 600 °C–700 °C [9]. A very recent model proposed by Xu *et al* [17], and supported by experimental data explains convincingly how the presence of ZrO_2 leads to a higher Sn contents in the Nb_3Sn by suppressing the reaction rate at the Nb_3Sn/Nb-alloy interface. Just as in our work, higher upper critical fields were obtained in the samples based on Nb–Ta–Zr alloys with internal oxidation. Based on this we believe that there is very compelling evidence for this second hypothesis but a precise comparison/analysis of the Sn concentration in our samples is necessary for a full confirmation.

It remains to be fully understood how the Zr and its internal oxidation can further contribute to the achievement of the full potential of Nb_3Sn at high magnetic fields, potential that is still yet to be reached as also suggested by Zhou *et al* [22], whose high homogeneity bulk Nb_3Sn samples showed upper critical fields 'as high as any optimized Ta- or Ti-doped wire'. The current work clearly shows that the simultaneous presence of Ta, Zr and O can get us closer to reaching this full potential.

5. Conclusion

In this work we have confirmed that the internal oxidation of Zr leads to the refinement of Nb_3Sn grains and thus to an increase of the critical current density. We have also shown that CuO can be an alternative to SnO_2 as an oxygen source for the internal oxidation of Zr.

Probably because of a lower density of ZrO_2 nanoparticles as compared with the samples of Xu *et al* [8, 9], our samples do not show a significant shift to higher normalized magnetic fields of the pinning force maximum that would correspond to a contribution from a second pinning mechanism.

The grain refinement and the enhancement of the critical current density that were obtained by the internal oxidation of Zr in Nb_3Sn samples based on Nb–Ta–Zr alloys are similar with those obtained in samples based on Nb-1Zr.

The combined presence of Ta and Zr leads to a record value of 29.2 T at 4.2 K for the upper critical field determined with a criterion of 99% of the normal state resistance, in samples based on Nb-7.5 wt%Ta-2 wt%Zr. This represents an improvement of 1.3 T with respect to the values obtained in similar samples based on Nb-7.5Ta. Further experimental work is needed to check the effect of the heat treatment on this improvement and to verify the hypotheses that we have put forward to explain the combined presence of Ta, Zr and O can lead to this improvement.

The superiority in upper critical field of our samples based on Nb–Ta–Zr over those based on Nb-7.5Ta is present at all criteria, which means that this applies to the irreversibility field as well. Given that the widths of the superconducting transitions and the Sn content variations across the layer in these samples are comparable with those encountered in industrial powder-in-tube wires, we expect a similar enhancement of the critical magnetic fields in practical multifilamentary Nb_3Sn wires.

Based on the fact that Nb-7.5Ta-2Zr leads to better critical fields than Nb-7.5Ta-1Zr and that we have not performed other composition or heat treatment optimization studies, we can speculate that further enhancements of the upper critical field may be possible by the adjustment of the heat treatments and concentrations of Zr and Ta.

Acknowledgments

We thank Dr-Ing. Max Schlötter GmbH & Co. KG of Geislingen/Steige, Germany for supplying the electrolytic solutions used for electroplating. The Nb–Ta–Zr alloys were acquired from the Materials Preparation Center at Ames Laboratory, which is supported by the US DOE Basic Energy Sciences. The authors acknowledge the support of the LNCMI-CNRS, member of the European Magnetic Field Laboratory (EMFL). Financial support was provided by the Swiss National Science Foundation (Grant No.

200021_184940) and by the European Organization for Nuclear Research (CERN), Memorandum of Understanding for the FCC Study, Addendum FCC-GOV-CC-0112 (KE3646/ATS) and Addendum FCC-GOV-CC-0175 (KE4663/ATS).

ORCID iDs

F Buta https://orcid.org/0000-0002-7119-8427
M Bonura https://orcid.org/0000-0002-8512-0989
D Matera https://orcid.org/0000-0002-9353-1497
G Bovone https://orcid.org/0000-0002-9161-7828
A Ballarino https://orcid.org/0000-0002-1705-4537
S C Hopkins https://orcid.org/0000-0002-0245-8627
B Bordini https://orcid.org/0000-0002-7122-623X
X Chaud https://orcid.org/0000-0002-3053-1350
C Senatore https://orcid.org/0000-0002-9191-5016

References

[1] Rossi L 2007 *IEEE Trans. Appl. Supercond.* **17** 1005–14
[2] Brünning O and Rossi L (eds) 2015 *The High Luminosity Large Hadron Collider* (Singapore: World Scientific) (https://doi.org/10.1142/9581)
[3] Benedikt M and Zimmermann F 2016 *J. Korean Phys. Soc.* **69** 893–902
[4] Ballarino A and Bottura L 2015 *IEEE Trans. Appl. Supercond.* **25** 6000906
[5] Ballarino A *et al* 2019 *IEEE Trans. Appl. Supercond.* **29** 1–9
[6] Xu X, Peng X, Rochester J, Lee J Y and Sumption M 2020 *Scr. Mater.* **186** 317–20
[7] Tachikawa K and Lee P 2012 *100 Years of Superconductivity* ed H Rogalla and P H Kes (Boca Raton, FL: CRC Press) pp 661–9
[8] Xu X, Sumption M, Peng X and Collings E W 2014 *Appl. Phys. Lett.* **104** 082602
[9] Xu X, Sumption M D and Peng X 2015 *Adv. Mater.* **27** 1346–50
[10] Benz M G 1968 *Trans. Met. Soc. AIME* **242** 1067–70
[11] Rumaner L E, Benz M G and Hall E L 1994 *Metall. Mater. Trans.* A **25** 213–9
[12] Zeitlin B A, Gregory E, Marte J, Benz M, Scanlan R and Dietderich D 2006 *AIP Conf. Proc.* **824** 513–9
[13] Zeitlin B A, Gregory E, Marte J, Benz M, Tae P, Scanlan R and Dietderich D 2005 *IEEE Trans. Appl. Supercond.* **15** 3393–8
[14] Motowidlo L R, Lee P J, Tarantini C, Balachandran S, Ghosh A K and Larbalestier D C 2018 *Supercond. Sci. Technol.* **31** 014002
[15] Xu X 2017 *Supercond. Sci. Technol.* **30** 093001
[16] Xu X, Rochester J, Peng X, Sumption M and Tomsic M 2019 *Supercond. Sci. Technol.* **32** 02LT1
[17] Xu X, Sumption M D, Lee J, Rochester J and Peng X 2020 *J. Alloys Compd.* **845** 156182
[18] Balachandran S, Tarantini C, Lee P J, Kametani F, Su Y F, Walker B, Starch W L and Larbalestier D C 2019 *Supercond. Sci. Technol.* **32** 044006
[19] Suenaga M and Sampson W B 1972 *Appl. Phys. Lett.* **20** 443–5
[20] Bean C P 1964 *Rev. Mod. Phys.* **36** 31–39
[21] Kim Y B, Hempstead C F and Strnad A R 1963 *Phys. Rev.* **129** 528–35
[22] Zhou J, Jo Y J, Sung Z H, Zhou H D, Lee P J and Larbalestier D C 2011 *Appl. Phys. Lett.* **99** 122507
[23] Eikelboom J A, Hartmann R A and Van De Klundert L J M 1989 *IEEE Trans. Magn.* **25** 1968–71
[24] Godeke A, Jewell M C, Fischer C M, Squitieri A A, Lee P J and Larbalestier D C 2005 *J. Appl. Phys.* **97** 093909
[25] Veringa H, Hoogendam P and Wees A 1983 *IEEE Trans. Magn.* **19** 773–6
[26] Hawes C D, Lee P J and Larbalestier D C 2006 *Supercond. Sci. Technol.* **19** S27–S37
[27] Di Michiel M and Scheuerlein C 2007 *Supercond. Sci. Technol.* **20** L55–L58
[28] Nazareth V R, Sumption M D, Peng X, Gregory E, Tomsic M J and Collings E W 2008 *AIP Conf. Proc.* **986** 260–8
[29] Xu X 2016 PhD Dissertation The Ohio State University (http://rave.ohiolink.edu/etdc/view?acc_num=osu1461071733)
[30] Scheuerlein C, Di Michiel M, Arnau Izquierdo G and Buta F 2008 *IEEE Trans. Appl. Supercond.* **18** 1754–60
[31] Scheuerlein C, Di Michiel M, Arnau G, Flükiger R, Buta F, Pong I, Oberli L and Bottura L 2011 *IEEE Trans. Appl. Supercond.* **21** 2554–8
[32] Dew-Hughes D 1974 *Phil. Mag.* **30** 293–305
[33] Buta F 2021 (unpublished)
[34] Suenaga M, Welch D O, Sabatini R L, Kammerer O F and Okuda S 1986 *J. Appl. Phys.* **59** 840–53
[35] Tarantini C, Segal C, Sung Z, Lee P, Oberli L, Ballarino A, Bottura L and Larbalestier D 2015 *Supercond. Sci. Technol.* **28** 095001
[36] Baumgartner T, Hecher J, Bernardi J, Pfeiffer S, Senatore C and Eisterer M 2017 *Supercond. Sci. Technol.* **30** 014011
[37] Godeke A 2006 *Supercond. Sci. Technol.* **19** R68–R80
[38] Ten Haken B, Godeke A and Ten Kate H H J 1995 *IEEE Trans. Appl. Supercond.* **5** 1909–12
[39] Godeke A, Jewell M C, Golubov A A, Haken B T and Larbalestier D C 2003 *Supercond. Sci. Technol.* **16** 1019–25
[40] Katagiri K, Okada T, Walters C R and Ekin J W 1995 *Cryogenics* **35** S85–S88
[41] Ten Haken B, Godeke A and Ten Kate H H J 1999 *J. Appl. Phys.* **85** 3247–53
[42] Seeber B, Uglietti D, Abächerli V, Bovier P A, Eckert D, Kübler G, Lezza P, Pollini A and Flükiger R 2005 *Rev. Sci. Instrum.* **76** 093901
[43] Seeber B, Senatore C, Buta F, Flükiger R, Boutboul T, Scheuerlein C, Oberli L and Rossi L 2008 *WAMSDO Workshop Accelerator Magnet Superconductors, Design and Optimization* ed E Todesco (Geneva: CERN) pp 37–41
[44] Lu X F and Hampshire D P 2009 *Supercond. Sci. Technol.* **23** 025002
[45] Bordini B, Bottura L, Mondonico G, Oberli L, Richter D, Seeber B, Senatore C, Takala E and Valentinis D 2012 *IEEE Trans. Appl. Supercond.* **22** 6000304

[46] Peng X, Gregory E, Tomsic M, Sumption M D, Ghosh A, Lu X F, Cheggour N, Stauffer T C, Goodrich L F and Splett J D 2011 *IEEE Trans. Appl. Supercond.* **21** 2559–62
[47] Akihama R, Yasukochi K and Ogasawara T 1977 *IEEE Trans. Magn.* **13** 803–6
[48] Bormann R, D Y Y, Hammond R, Geballe T, Foner S and McNiff E 1985 *IEEE Trans. Magn.* **21** 1140–3
[49] Suenaga M, Ghosh A K, Xu Y and Welch D O 1991 *Phys. Rev. Lett.* **66** 1777–80
[50] Zheng D N, Ingle N J C and Campbell A M 2000 *Phys. Rev.* B **61** 15429–35
[51] Cooley L D, Fischer C M, Lee P J and Larbalestier D C 2004 *J. Appl. Phys.* **96** 2122–30
[52] Kramer E J 1973 *J. Appl. Phys.* **44** 1360–70
[53] Fischer C M 2002 MSc Thesis University of Wisconsin-Madison (https://fs.magnet.fsu.edu/∼lee/asc/pdf_papers/theses/cmf02msc.pdf)
[54] Fischer C M, Lee P J and Larbalestier D C 2002 *AIP Conf. Proc.* **614** 1008–15
[55] Hechler K, Horn G, Otto G and Saur E 1969 *J. Low Temp. Phys.* **1** 29–43
[56] He B, Dong C, Cao W, Liao C, Yang L and Chen H 2010 *Supercond. Sci. Technol.* **23** 025016
[57] Takeuchi T, Asano T, Iijima Y and Tachikawa K 1981 *Cryogenics* **21** 585–90